The Astrophysical Journal, 961:212 (11pp), 2024 February 1 https://doi.org/10.3847/1538-4357/ad02f0
© 2024. The Author(s). Published by the American Astronomical Society.
OPEN ACCESS

Collapsar Gamma-Ray Bursts Grind Their Black Hole Spins to a Halt

Jonatan Jacquemin-Ide, Ore Gottlieb, Beverly Lowell, and Alexander Tchekhovskoy
Center for Interdisciplinary Exploration & Research in Astrophysics (CIERA), Physics & Astronomy, Northwestern University, Evanston, IL 60202, USA
jonatan.jacqueminide@northwestern.edu
Received 2023 February 20; revised 2023 October 9; accepted 2023 October 11; published 2024 January 29

Abstract

The spin of a newly formed black hole (BH) at the center of a massive star evolves from its natal value due to two competing processes: accretion of gas angular momentum that increases the spin and extraction of BH angular momentum by outflows that decreases the spin. Ultimately, the final, equilibrium spin is set by a balance between both processes. In order for the BH to launch relativistic jets and power a γ-ray burst (GRB), the BH magnetic field needs to be dynamically important. Thus, we consider the case of a magnetically arrested disk (MAD) driving the spin evolution of the BH. By applying the semianalytic MAD BH spin evolution model of Lowell et al. to collapsars, we show that if the BH accretes $\sim$20% of its initial mass, its dimensionless spin inevitably reaches small values, $a \lesssim 0.2$. For such spins, and for mass accretion rates inferred from collapsar simulations, we show that our semianalytic model reproduces the energetics of typical GRB jets, $L_{\rm jet} \sim 10^{50}$ erg s^{-1}. We show that our semianalytic model reproduces the nearly constant power of typical GRB jets. If the MAD onset is delayed, this allows powerful jets at the high end of the GRB luminosity distribution, $L_{\rm jet} \sim 10^{52}$ erg s^{-1}, but the final spin remains low, $a \lesssim 0.3$. These results are consistent with the low spins inferred from gravitational wave detections of binary BH mergers. In a companion paper by Gottlieb et al., we use GRB observations to constrain the natal BH spin to be $a \simeq 0.2$.

Unified Astronomy Thesaurus concepts: Gamma-ray bursts (629); Astrophysical black holes (98); Relativistic jets (1390); Accretion (14)

1. Introduction

Black holes (BHs) are the product of a massive star core collapse at the end of its life (collapsar; Woosley 1993). Before the formation of the BH, the stellar core can undergo an intermediate stage during which it collapses into a proto–neutron star (PNS). The large mass reservoir in the stellar core leads to a high mass accretion rate onto the PNS. Once the PNS accretes mass above $M_{\rm NS,max} \gtrsim 2.2\,M_\odot$ (Margalit & Metzger 2017; Aloy & Obergaulinger 2021; Obergaulinger & Aloy 2022), it collapses to a BH. Observationally, the least massive observed BHs are $M_{\rm min} \simeq 2M_{\rm NS,max}$, suggesting the presence of a mass gap between $M_{\rm NS,max}$ and $M_{\rm min}$ (Bailyn et al. 1998; Özel et al. 2010; Farr et al. 2011; Mandel et al. 2017). Such a gap implies that after their formation and while the stellar collapse is ongoing, BHs continue to accrete mass that is at least comparable to their natal mass, $M_{\rm NS,max}$ (Belczynski et al. 2012; Kovetz et al. 2017). We note that the detection of the binary merger GW190814 of a 23 $M_\odot$ BH with a 2.6 $M_\odot$ compact object, casts doubt on the existence of the mass gap (Abbott et al. 2020).

As it accretes gas, the BH gains mass and angular momentum, so that its spin can either increase by accretion or decrease by generating collimated Poynting-flux-dominated outflows (jets) that extract BH rotational energy (Penrose & Floyd 1971). Numerical simulations of rotating collapsars have shown that in the absence of collimated outflows or jets (Shapiro & Shibata 2002; Shibata & Shapiro 2002; Fujibayashi et al. 2020, 2023), or if the jets are powered hydrodynamically, rather than by the rotational energy of the BH (MacFadyen & Woosley 1999; Janiuk et al. 2008), the BH spins up by the end of the explosion process to a dimensionless spin $a \approx 1$ (see however, Chan et al. 2018). We are unaware of numerical studies that consider both spin up by accretion and spin down by jet launching.

Several observational techniques have been used over the years to constrain the spin of BHs via electromagnetic (EM) emission of the BH accretion disk, from X-ray reflection spectroscopy (e.g., García et al. 2014) to thermal continuum fitting (e.g., Zhang et al. 1997; McClintock et al. 2014; Zhu et al. 2019). Although these methods suggest that at least some of the BHs are rapidly spinning, these measurements may depend on the poorly understood accretion physics of BHs (see Middleton 2016; Reynolds 2021, for reviews). A relatively new and more robust technique to infer the BH spin is through gravitational wave detections of binary BH mergers by LIGO–Virgo–KAGRA (LVK). Such studies consistently indicate that premerger BHs are slowly spinning (Farr et al. 2017; Tiwari et al. 2018; Roulet & Zaldarriaga 2019; Abbott et al. 2020; Hoy et al. 2022).

Some of the massive progenitors of BHs are stripped-envelope stars (e.g., Gal-Yam et al. 2022). These stars are associated with the detection of γ-ray bursts (GRBs), powered by relativistic jets launched from the BH. The enormous energy of those jets indicates that they are powered electromagnetically (e.g., Lyutikov & Blandford 2003; Leng & Giannios 2014; Liu et al. 2015) via the extraction of BH rotational energy by the magnetic fields threading the BH (BZ; Blandford & Znajek 1977). Therefore, jetted explosions link the birth of BHs and their spin with the formation of relativistic jets in the stellar core, providing a unique opportunity to study BHs through the observables of GRBs. In a companion paper by Gottlieb et al. (2023), we argue that GRB observables favor BHs with low natal spins. Here, we analyze the interplay

Original content from this work may be used under the terms of the Creative Commons Attribution 4.0 licence. Any further distribution of this work must maintain attribution to the author(s) and the title of the work, journal citation and DOI.

between the BH spin and the jet to study the BH spin evolution, and the final spin at the end of the stellar collapse.

A spinning BH exchanges angular momentum with its disk–jet accretion system, which results in both hydrodynamic torques through accretion and magnetic torques through jet launching acting on the BH. This continues until the BH reaches equilibrium spin. In order for the jets to be launched, the BH needs to possess dynamically important magnetic fields (Komissarov & Barkov 2009). BHs in this state are in or near the magnetically arrested disk (MAD) state (Bisnovatyi-Kogan & Ruzmaikin 1974, 1976; Narayan et al. 2003; Tchekhovskoy et al. 2011). Recently, Lowell et al. (2023) used the simulations of Tchekhovskoy et al. (2011, 2012) to compute the torques applied by the MAD system to a spinning BH. They constructed a semianalytic model that could reproduce the behavior of the magnetohydrodynamic torques of MADs on BHs. They found that MADs spin down BHs to a relatively low equilibrium spin, $a_{\rm eq} \simeq 0.07$, more efficiently than the spin up by a standard thin disk (Bardeen 1970). For example, an initially maximally spinning BH of $a_0 = 1$ can reach the equilibrium spin, $a_{\rm eq} \simeq 0.07$, by accreting only 50% of its initial mass during the MAD state. By contrast, for a standard thin disk, a minimally spinning BH, $a_0 = 0$, needs to accrete $\sim$200% of its initial mass to reach the equilibrium spin, $a = 1$.

The natal BH spin is a critical parameter of any spin-down model. It can be constrained using stellar evolution models, e.g., Fuller & Ma (2019) and Belczynski et al. (2020) found that newly formed BHs are born with a very low spin, $a \sim 10^{-2}$ if angular momentum transport in the star is efficient. The presence of the magnetic Taylor instability could lead to efficient angular momentum within the star. Thus, a strong coupling between the stellar core and the envelope results in weakly spinning BHs. Furthermore, one can estimate the BH spin from the collapse of a millisecond PNS as

$$a \simeq 0.03 \left(\frac{R_{\rm NS}}{10\ {\rm km}}\right)^2 \frac{1{\rm ms}}{P} \frac{3\,M_\odot}{M_{\rm NS,max}}\,, \tag{1}$$

where $R_{\rm NS}$ is the PNS radius and P is the PNS spin period. This estimate is consistent with low initial spins. The parameters of Equation (1) depend on the equation of state and the stellar angular momentum. Depending on those quantities the initial BH spin could take higher values. Obergaulinger & Aloy (2022) found that the PNS collapses into a BH with moderate spin, $a \sim 0.3$. Their results of higher spins originate in stellar models with inefficient angular momentum transport compared with the models discussed above which featured low spin.

In this paper, we build on the model of Lowell et al. (2023) to show that the final spin of collapsar BHs associated with Poynting-flux-dominated jets is almost inevitably small. In Section 2 we outline the reasoning why BHs end up slowly spinning at the end of stellar collapse. In Section 3 we present a semianalytic model of BH spin evolution. In Section 4 we compare the model with GRB observables to show that for any reasonable stellar collapse scenario, BHs spin down/up to an equilibrium spin of $a \approx 0.1$. In Section 5 we discuss the limits of our model. We summarize and conclude in Section 6.

2. Low Final BH Spin in a Nutshell

The angular momentum exchange between the BH, the disk, and the jets leads to magnetohydrodynamic torques on the BH. On the one hand, the infalling matter carries angular momentum inward and applies positive, spin-up, hydrodynamic torques to the BH. On the other hand, the accreting matter advects magnetic fields onto the BH: the magnetic flux threading the BH powers relativistic jets that apply negative, spin-down, EM torques to the BH.

In the MAD state, the jet power and EM torque are linked to the accretion power by the jet efficiency, which in turn depends on the BH spin (Lowell et al. 2023). Hence, the torques acting on the BH depend only on the accretion rate and the BH spin (Gottlieb et al. 2023). Consequently, the final BH spin depends solely on the initial BH spin, a_0, and the total accreted mass, m_f. We normalize the total accreted mass by the BH initial mass, $M_0 \equiv M(t=0)$, to define

$$\chi \equiv \frac{m_f}{M_0}. \tag{2}$$

We can also express the total accreted mass as an integral of the mass accretion rate, $\dot{m}$

$$m_f = \int_0^\infty \dot{m} {\rm d}t\ . \tag{3}$$

We note that χ does not represent the mass growth of the BH, but the total accreted mass on the BH. The increment in BH mass is lower than the accreted mass because some of the accreted energy is carried away by the relativistic jets and outflows, thus typically we have, $\chi > \frac{M(t\to\infty)}{M_0}$. For a sufficiently high accreted mass fraction, e.g., $\chi \gtrsim \frac{1}{2}$, the final BH spin reaches equilibrium spin, $a_f \simeq a_{\rm eq} = 0.07$ (Lowell et al. 2023). Ultimately, the accreted mass is likely related to the stellar mass $M_\star$. Thus, we define

$$\lambda \equiv \frac{m_f}{M_\star}. \tag{4}$$

One might naively expect most of the stellar envelope to fall onto the BH. However, the powerful jets and disk outflows will unbind a considerable fraction of the stellar envelope.

The percentage of the stellar envelope that is accreted by the BH was estimated by Gottlieb et al. (2022b) by measuring the percentage of mass that remains bound at the end of the simulation. They found that $\sim$20 s after the collapse, λ reaches an asymptotic value of $\lambda \approx 0.1$, e.g., 10% of the stellar mass will be accreted onto the BH. For such accretion fraction, a stellar envelope of 20 $M_\odot$ and an initial BH mass of 2.5 $M_\odot$ result in $\chi = 0.8$, as roughly needed for explaining the mass gap, well above the critical value for reaching equilibrium spin.

To compute the BH spin evolution in time, we model the BH spin by coupling the spin evolution equations to an imposed accretion rate (Moderski & Sikora 1996; Lowell et al. 2023)

$$\frac{1}{\dot{m}}\frac{{\rm d}a}{{\rm d}t} = \frac{s_{\rm MAD}(a)}{M}\,, \tag{5}$$

$$\frac{1}{\dot{m}}\frac{{\rm d}M}{{\rm d}t} = e_{\rm HD} - \eta_{\rm EM}(a)\,, \tag{6}$$

where the spin-up parameter can be written as

$$s_{\rm MAD}(a) = (l_{\rm HD} - 2a e_{\rm HD}) - \eta_{\rm EM}(a)\left(\frac{1}{k(a)\Omega_{\rm H}} - 2a\right), \tag{7}$$

where M is the mass of the BH, ${\rm d}m = \dot{m}{\rm d}t$ is the accreted mass, $\eta_{\rm EM}(a)$ is the jet launching efficiency, $e_{\rm HD}$ and $l_{\rm HD}$ are the hydrodynamic energy and angular momentum fluxes,

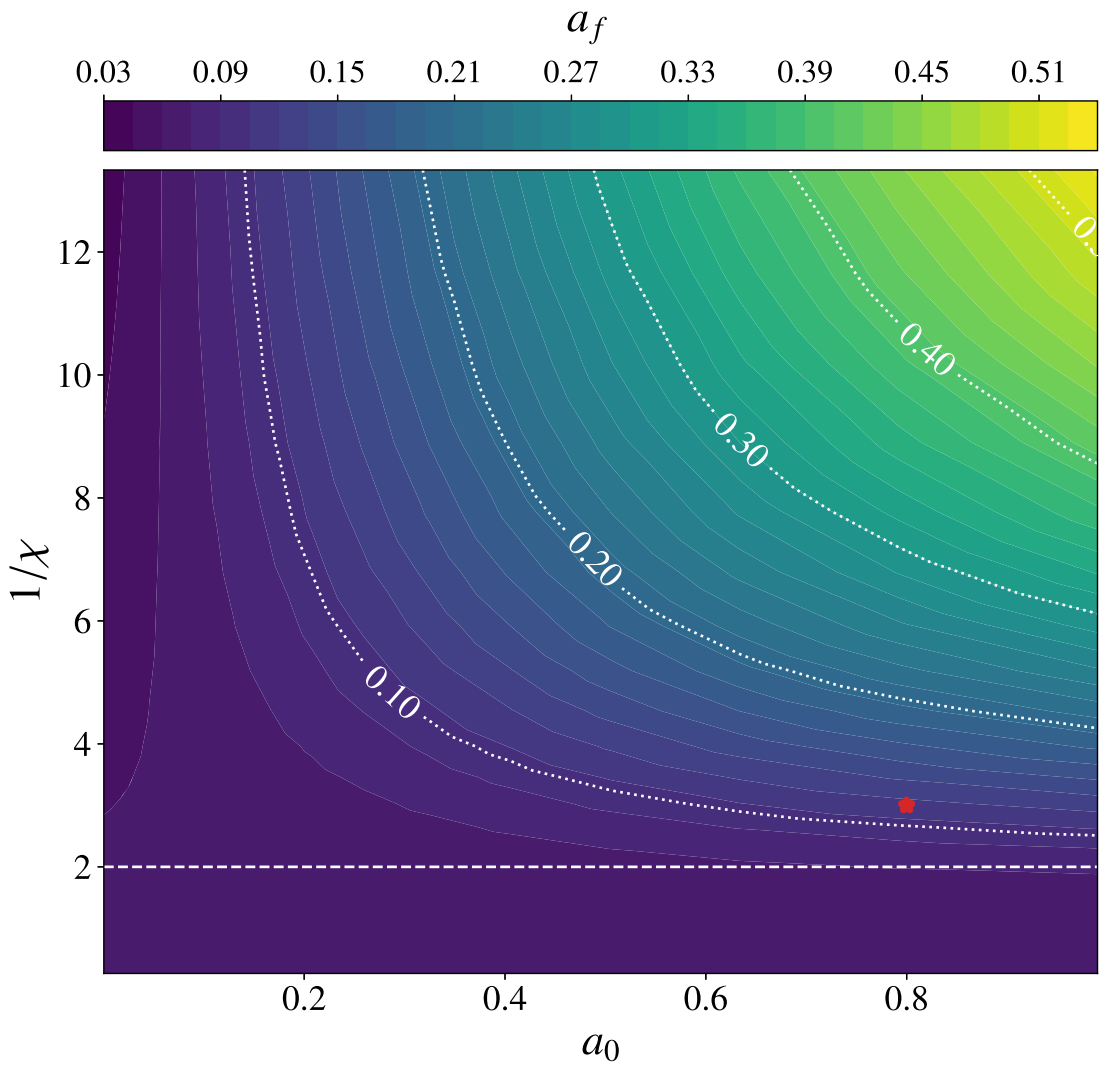

Figure 1. Final spin of the BH as a function of the inverse of the accreted mass, $1/\chi$ (Equation (2)), and the initial BH spin a_0. All BHs that accrete more than half of their original mass, i.e., $1/\chi < 2$ showed by the white dashed line, spin down to equilibrium spin, $a_{\rm eq} \simeq 0.07$. The simulation of Gottlieb et al. (2022b) with initial spin $a_0 = 0.8$ and $\chi \simeq 0.3$ is marked by the red star. Most BHs spin down to $a \leqslant 0.3$ as long as they accrete 15% of their initial mass, irrespective of their initial spin.

respectively, and $k(a) = \Omega_{\rm F}/\Omega_{\rm H}$ is the angular frequency of the magnetic field lines over the angular frequency of the event horizon. The numerical values of $e_{\rm HD}$ and $l_{\rm HD}$, and the functions $\eta_{\rm EM}(a)$ and $k(a)$ are taken from Lowell et al. (2023).[1]

The jet power is dictated by the mass accretion rate $\dot{m}$ and jet launching efficiency $\eta_{\rm EM}$, which in turn depend solely on the BH spin (Lowell et al. 2023)

$$L_{\rm jet} = \eta_{\rm EM}(a)\dot{m}c^2 \,. \tag{8}$$

The jet power does not explicitly depend on the magnetic field, because in the MAD the magnetic field can be explicitly expressed as a function of the accretion rate (Tchekhovskoy et al. 2011). Typically, high accretion rates, like the ones in collapsars, will lead to high magnetic fields at the horizon, $B > 10^{15}$ G.

Figure 1 depicts the final BH spin from multiple spin-down solutions computed with different initial BH spins a_0, and total accreted mass χ. All solutions with $1/\chi < 2$ reach equilibrium spin, $a_{\rm eq} = 0.07$, as was found by Lowell et al. (2023). The spin down is also efficient for lower values of accreted mass. For example, even for a small total accreted mass of 0.2 M_0, i.e., $1/\chi = 5$, the final BH spin is $a_f \lesssim 0.2$. The simulation of Gottlieb et al. (2022b) with an initial spin $a_0 = 0.8$ and $\chi \simeq 0.3$, marked by the red star in Figure 1, should reach $a_f \simeq 0.1$. This demonstrates that even if the natal BH spin is high and χ is below the critical value of $\chi = 0.5$, the spin down is substantial. We conclude that for any reasonable accreted mass, e.g., $m_f \sim 1\,M_\odot$, collapsar BHs inevitably spin down to low spins of $a_f \approx 0.1$, independent of the mass accretion rate.

The efficient spin down is a result of multiple compounding torques in MADs. First, MAD jets extract angular momentum more efficiently than the monopolar BZ model predicts. These higher torques are due to a lower angular frequency of the magnetic field rotation, $\Omega_{\rm F}$, parameterized with $k(a) = \Omega_{\rm F}/\Omega_{\rm H}$, where $\Omega_{\rm H}$ is the event horizon angular frequency. The monopolar BZ model has $k(a) = 0.5$, and the parabolic BZ model has $k(a) \simeq 0.3$ near the jet edge where most of the power comes out (see Figure 4 in Tchekhovskoy et al. 2010). Lowell et al. (2023) measure values of $k < 0.35$ for all spins and even lower for lower spins, i.e., closer to the parabolic rather than

[1] We note that in Lowell et al. (2023) the spin evolution was computed using interpolation between simulation values of s, while in our work we use their analytic model. This leads to small differences in the spin evolution.

monopolar BZ model. Second, the strong magnetic field anchored in the disk induces powerful Blandford & Payne (1982) torques that reduce the net angular momentum of the disk (Lowell et al. 2023). As a result, the accreted hydrodynamic angular momentum, $l_{\rm HD}$, is smaller than the one predicted by Bardeen (1970) by a factor of $\sim$2. Consequently, the BH is starved of angular momentum, leading to a more efficient spin down.

The parameters and functionals of the spin-down model ($\eta_{\rm EM}(a)$, $k(a)$, $e_{\rm HD}$, and $l_{\rm HD}$) were computed by Lowell et al. (2023) using GRMHD numerical simulations. Great care was taken to remove the artificial density floors from the hydrodynamic energy and angular momentum fluxes. The computation of the magnetic functionals ($k(a)$ and $\eta_{\rm EM}(a)$) is simpler since they are not affected by artificial floors. It was then verified that the parameters ($\eta_{\rm EM}(a)$, $k(a)$, $e_{\rm HD}$, and $l_{\rm HD}$) could reproduce the independent (direct) measurement of $s_{\rm MAD}$ (see their Figure 5). We note that Narayan et al. (2022) computed a spin-down parameter that is very similar to ours, with a relative difference of $\lesssim$30%. However, their equilibrium spin of 0.035 is about half of that found in Lowell et al. (2023). This discrepancy could be attributed to the different sampling close to $a_{\rm eq}$.

We stress that the spin evolution model of Lowell et al. (2023) is only valid for an engine that has reached the MAD state and is radiatively inefficient. We verify that the spin evolution model of Lowell et al. (2023) is valid for collapsars by showing that it is compatible with the spin-up parameter in collapsar simulations with $a = 0.8$ and $a = 0.1$ (see Appendix A). In collapsar simulations the system reaches the MAD state relatively fast, $t < 1$ s (see Appendix A). However, the system could take longer to reach the MAD state with different initial conditions, as discussed in Section 4.2.

3. BH Spin Evolution

The magnitude and time dependence of the accretion onto the BH depend on the stellar mass and density profile, respectively. 1D core-collapse simulations and self-similar models find that density profiles from stellar evolution models, $\rho(r) \propto r^{-2.5}$, flatten prior to the BH formation to $\rho(r) \propto r^{-1.5}$ (Halevi et al. 2023).[2] For freefall of a typical stellar envelope mass, numerical and analytic results show that this power law leads to a steady BH accretion of $\dot{m} \gtrsim 10^{-2}\ M_\odot\ {\rm s}^{-1}$ (Gottlieb et al. 2022b, 2023). If we were to extrapolate that rate to typical GRB durations of a few dozens of seconds, the BH would accrete $m_f \approx 1\ M_\odot$. For $M_0 \simeq M_{\rm NS,max}$, this corresponds to a 50% increase in the BH mass and final spin $a_f \simeq a_{\rm eq}$.

For a roughly constant accretion rate until time t_f, we adopt the following time-dependency of $\dot{m}$

$$\dot{m} = \dot{m}_0 \frac{1}{1 + e^{t - t_f}}, \tag{9}$$

where

$$t_f = \ln\left(e^{\frac{M_\star \lambda}{\dot{m}_0}} - 1\right) \simeq \frac{m_f}{\dot{m}}, \tag{10}$$

is the characteristic accretion duration, the time where the mass reservoir, $m_f = M_\star \lambda$, has been exhausted. For simplicity, we adopt a constant $\dot{m}$. In our model, the mass-depletion timescale, t_f, is a free parameter computed using Equation (10) for a choice of $\dot{m}_0$ and m_f. We note that a constant accretion rate is not strictly consistent with the simulations of Gottlieb et al. (2023), which feature a small decrease of $\dot{m}$ with time. Furthermore, the asymptotic behavior of $\dot{m}$ is not constrained, as discussed in Section 6.

We can recover the argument in Section 2 using the accretion rate timescale t_f and the spin-down timescale $t_{\rm spin}$. In MADs, the magnetic field scales as $B \propto \sqrt{\dot{m}}$, leading to $L_{\rm jet} \propto \dot{m}$. This implies that the spin-down timescale due to the jet torque is inversely[3] proportional to the accretion rate. This can be shown from Equation (5), which dictates that the spin-down timescale is

$$t_{\rm spin} = \frac{a}{-\frac{{\rm d}a}{{\rm d}t}} \sim \frac{M_0}{\dot{m}} \frac{a_0}{|s_{\rm MAD}(a_0)|}. \tag{11}$$

Note that this timescale is independent of the magnetic field and the jet power. Comparing $t_{\rm spin}$ with the accretion timescale

$$\frac{t_{\rm spin}}{t_f} \simeq \frac{1}{\chi} \frac{a_0}{|s_{\rm MAD}(a_0)|}, \tag{12}$$

we find that for initial spins far from the equilibrium spin, $a_0 > 0.2$, we get $\frac{a_0}{|\,s_{\rm MAD}(a_0)\,|} \leqslant 0.2$. Thus, for $\chi \geqslant 0.2$ we expect for the BH to spin down considerably before $t = t_f$, consistent with Section 2.

Figure 2 demonstrates the evolution of the BH mass (a) and spin (b) for different initial spins, where $t = 0$ is the MAD state activation time, assuming $\lambda = 0.2$ and $\chi = 1.2$. The BH mass saturates once the accretion stops, denoted by t_f, whereas the BH spin saturates when $a = a_{\rm eq}$, before t_f. All solutions converge to equilibrium spin, with lower initial spins reaching $a_f = a_{\rm eq}$ faster. The final BH mass is practically independent of the initial spin.

4. Observables of the Spin-down Model

We examine the compatibility of our semianalytic solution with the observed GRB characteristics: duration t_f, average luminosity $\langle L_{\rm jet} \rangle$ (Equation (15)), and time evolution $R_{L_{\rm jet}}$ (Equation (16)).

To compute the GRB characteristics, we model the jet propagation inside the star with the semianalytic model of Harrison et al. (2018), which relies on the formalism of hydrodynamic jets (Bromberg et al. 2011; see the caveats in Section 6). We adopt the following mass density profile in the star

$$\rho \equiv \rho_0 \left(\frac{r}{r_H}\right)^{-1.5} \left(1 - \frac{r}{R_\star}\right)^3, \tag{13}$$

where r_H is the radius of the BH and $R_\star$ is the radius of the star. The density ρ_0 is normalized using the total mass of the star, $M_\star$. Using the jet power from our engine evolution model and the above stellar profile, we compute the jet propagation within the stellar envelope and the breakout time t_b. The jet power at the jet head is computed using the retardation time, $t - z_h/c$, where z_h is the position of the jet head. The cumulative energy carried by the jet is approximated to be the jet energy that does

[2] See also Bethe (1990) for a similar result in a semianalytic limit.

[3] A higher B field would result in a higher torque and a shorter spin-down timescale.

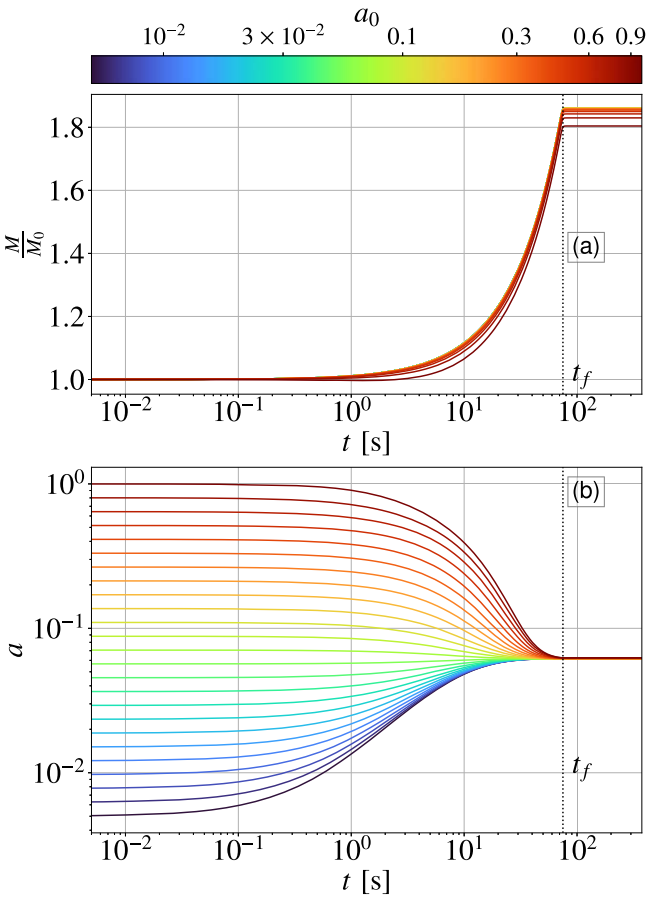

Figure 2. Evolution of $a(t)$ (panel (a)) and $\frac{M}{M_0}(t)$ (panel (b)) as functions of time and different initial spins $a_0 \in [5\times10^{-3}, 1.0]$. The time at which accretion stops, t_f, is shown by the vertical dotted line. All solutions were obtained for $\dot{m} = 3\times10^{-2}\ M_\odot\ \mathrm{s}^{-1}$, $\lambda = 0.2$, $M_\star = 15\ M_\odot$, $M_0 = 2.5\ M_\odot$, and $\chi = 1.2$. Smaller spins reach spin equilibrium faster than higher spins.

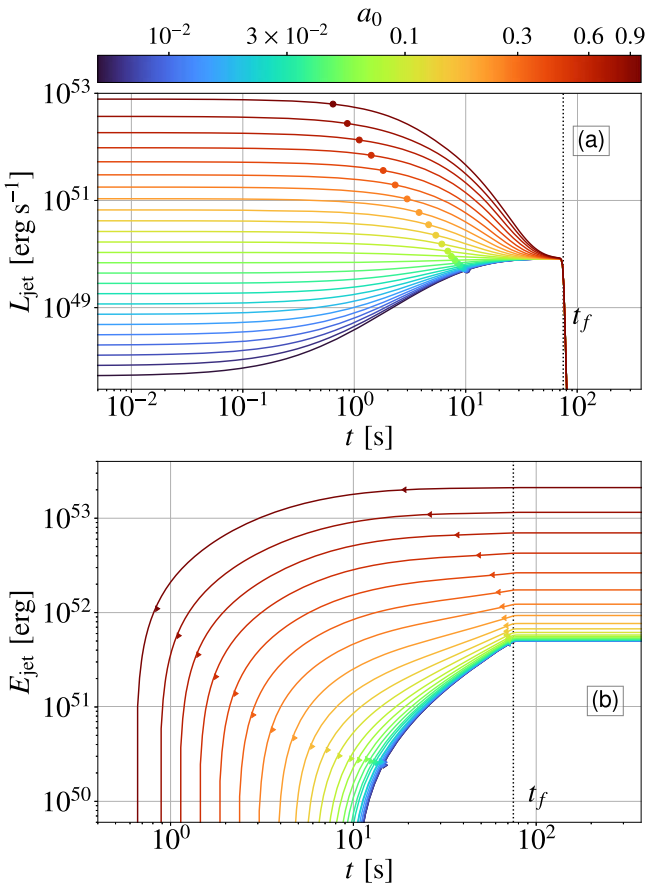

Figure 3. Evolution of $L_{\rm jet}$ (panel (a)) and $E_{\rm jet}$ (panel (b)) as functions of time and different initial spins, $a_0 \in [5\times10^{-3}, 1.0]$. The circles in panel (a) mark $t_b - \frac{R_\star}{c}$, which is the time after which unshocked jet elements can emerge from the star. The left and right triangles in panel (b) represent t_1 and t_2, respectively. The vertical dotted line marks the time at which accretion stops t_f. All solutions are computed using $\dot{m} = 3\times10^{-2}\ M_\odot\ \mathrm{s}^{-1}$, $\lambda = 0.2$, $M_\star = 15\ M_\odot$, $R_\star = 1\ R_\odot$, $M_0 = 2.5\ M_\odot$, and $\chi = 1.2$.

not cross the reverse shock before breakout

$$E_{\rm jet}(t) = \int_{t_b - R_\star/c}^{t} L_{\rm jet} dt. \tag{14}$$

We then define t_1 and t_2, which are the times when 5% and 95% of the jet energy has been released, respectively. Thus, 90% of the jet energy is released in the timescale $T_{90} = t_2 - t_1$. To represent the characteristic jet power of every solution, we define the average jet power

$$\langle L_{\rm jet}\rangle \equiv \frac{1}{T_{90}}\int_{t_1}^{t_2} L_{\rm jet} dt\ . \tag{15}$$

To quantify the evolution of the jet power, we define the ratio

$$R_{L_{\rm jet}} = \left| \frac{\max\left(L_{\rm jet}(t_1 \leqslant t \leqslant t_2)\right)}{\min\left(L_{\rm jet}(t_1 \leqslant t \leqslant t_2)\right)} \right|\ . \tag{16}$$

We impose $R_{L_{\rm jet}} \leqslant 2.5$ so that the jet power remains roughly constant during the GRB's duty cycle (e.g., McBreen et al. 2002).

4.1. BH Spin Evolution of Typical GRBs

To obtain the characteristic GRB jet power, one needs to consider the highly uncertain γ-ray radiative efficiency ϵ_γ. We choose a fiducial value of $\epsilon_\gamma = 0.5$, so the jet power and energy are $L_{\rm jet} = L_{\rm jet,obs}/\epsilon_\gamma$ and $E_{\rm jet} = E_{\rm jet,obs}/\epsilon_\gamma$, respectively. The typical range of the GRB jet luminosity and energy are $6\times10^{49}\ \mathrm{erg\ s^{-1}} \leqslant \langle L_{\rm jet}\rangle \leqslant 4\times10^{51}\ \mathrm{erg\ s^{-1}}$ and $3\times10^{50}\ \mathrm{erg} \leqslant \langle E_{\rm jet}\rangle \leqslant 6\times10^{51}$ erg, respectively (Goldstein et al. 2016).

Figure 3(a) delineates the evolution of the jet power and energy for different initial BH spins. We assume $\dot{m} = 3\times10^{-2}\ M_\odot\ \mathrm{s}^{-1}$, which is consistent with our choice of stellar profile and the values measured by Gottlieb et al. (2023). While higher initial spins lead to higher power and more energetic jets, all BHs reach an equilibrium spin within the typical long GRB duration. Consequently, all jets also converge to the same value, $L_{\rm jet} = \eta_{\rm EM}(a = a_{\rm eq})\times\dot{m}c^2 \simeq 8\times10^{49}\ \mathrm{erg\ s^{-1}}$, consistent with the typical GRB jet power. The unshocked jet element breakout time from the star, $t_b - \frac{R_\star}{c}$, marked by a filled circle, represents the time from which the time evolution in the jet power can be observed. If the BH spin is still evolving considerably at $t > t_b$, there will be visible variations in the observed jet power, in tension with observations. Figure 3(b) shows the jet energy, as calculated in Equation (14). The energy of all jets launched from BHs with initial spins of $a_0 \lesssim 0.1$ is dominated by the energy released when the BH reaches equilibrium spin, $L_{\rm jet}(a = a_{\rm eq})$, and converges to $E_{\rm jet} \approx 5\times10^{51}$ erg by the end of the GRB, at $t = t_f$. This jet energy is within 1σ of the observed jet energy distribution (Goldstein et al. 2016).

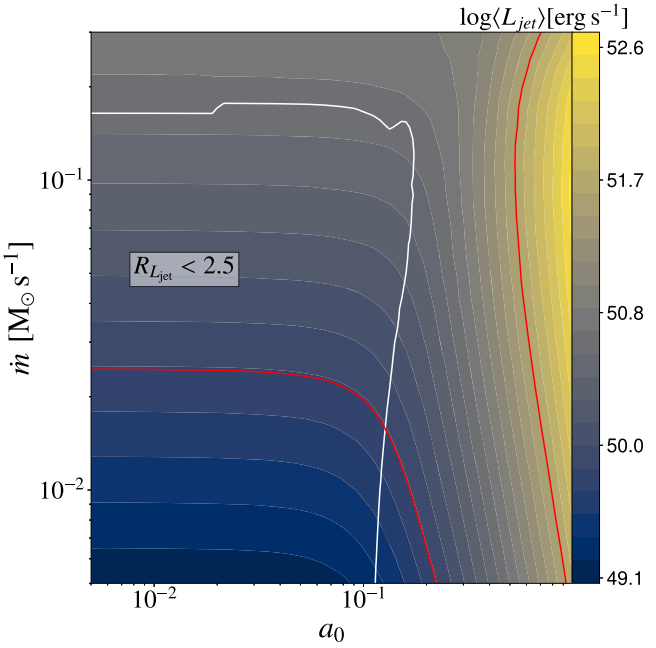

Figure 4. Jet power as a function of $\dot{m}$ and the BH initial spin. The area under the white contour constrains the emerging jets with minimum time evolution in their emission, characterized by $R_{L_{\rm jet}} \leqslant 2.5$. The red lines represent the observational 1σ spread around the average jet power (Goldstein et al. 2016). Only solutions with weak initial spins, $a_0 \leqslant 0.1$, and accretion rates of $2 \times 10^{-2}\ M_\odot\ \mathrm{s}^{-1} \gtrsim \dot{m} \gtrsim 1.5 \times 10^{-1}\ \mathrm{M}_\odot\ \mathrm{s}^{-1}$ are consistent with both constraints. All solutions are computed using $\lambda = 0.15$, $M_\star = 15\ M_\odot$, $R_\star = 1\ R_\odot$, $M_0 = 2.5\ M_\odot$, and $\chi = 0.9$. In this figure, the higher the $\dot{m}$ the lower the t_f as the accreted mass $m_f = \lambda M_\star$ is fixed and $t_f \sim m_f/\dot{m}$.

Figure 4 displays the dependence of the average jet luminosity on the mass accretion rate and initial spin. The average jet luminosity is governed by the more luminous phase of the jet. Thus, for low initial spins, $a_0 < a_{\rm eq}$, the average jet power does not depend on the initial spin, and depends only on the accretion rate. This is consistent with Figure 3(a), which shows that low spins quickly reach equilibrium spin, thus $L_{\rm jet} \approx \eta(a_{\rm eq})\dot{m}c^2$. This trend is reversed for high initial spins, $a_0 > a_{\rm eq}$, where the contour lines are primarily vertical, i.e., the average jet power is dictated by the jet luminosity when the BH spin is a_0.

Most BH spins and mass accretion rates are consistent within 1σ with the observed jet power, outlined by the red lines in Figure 4. The jet power obtained in the solutions under the white line varies by less than a factor of 2.5, as shown in Equation (16). Only solutions with low initial spins, $a_0 \lesssim 0.1$, reach equilibrium spin at $t < t_1$, and thus exhibit a flat jet power curve that could reproduce the observational data (Figure 3(a)).

For a mass accretion rate of $\dot{m} \gtrsim 10^{-2}\ M_\odot\ \mathrm{s}^{-1}$, a typical GRB jet power is obtained. If the mass accretion rate is $\dot{m} < 10^{-2}\ M_\odot\ \mathrm{s}^{-1}$, weaker jets with $\langle L_{\rm jet,obs}\rangle/\epsilon_\gamma \leqslant 6 \times 10^{49}$ erg emerge.

4.2. BH Spin of Powerful GRB Jets

Figure 4 shows that powerful GRBs with $L_{\rm jet}/\epsilon_\gamma \geqslant 5 \times 10^{51}$ erg s^{-1} are excluded from the variation constraint. Here we show that the most powerful GRB jets can emerge by delaying the activation of the MAD state (the jet launching). To investigate the effects of delaying the onset of the MAD state, we introduce the function $\Phi(t)$ that represents the disk state with respect to MAD

$$\Phi(t) = 1 - e^{-t/\,t_{\rm MAD}}\,, \tag{17}$$

where $t_{\rm MAD}$ is the characteristic time for the disk to become MAD. When $t \ll t_{\rm MAD}$, the disk acts as a standard viscously accreting hydrodynamic disk, and its torques on the BH are modeled with the standard theory of Bardeen (1970). We write a modified set of spin evolution equations that follow the spin evolution in Bardeen (1970) up until the system becomes MAD

$$\frac{1}{\dot{m}}\frac{{\rm d}a}{{\rm d}t} = \frac{s_{\rm MAD}(a)\Phi(t) + s_{\rm Ba}(1-\Phi(t))}{M}\,, \tag{18}$$

and

$$\frac{1}{\dot{m}}\frac{{\rm d}M}{{\rm d}t} = e_{\rm Ba}(1-\Phi(t)) + (e_{\rm HD} - \eta_{\rm EM}(a))\Phi(t)\,, \tag{19}$$

where $e_{\rm Ba}$ and $s_{\rm Ba}$ are taken from Bardeen (1970), and $s_{\rm MAD}$ is defined in Equation (7). We reintroduce the jet power in Equation (8) with the magnetic flux saturation parameter as

$$L_{\rm jet} = \Phi(t)\eta_{\rm EM}(a)\dot{m}c^2. \tag{20}$$

When $\Phi(t) = 1$, the magnetic field of the BH and inner disk have saturated and we recover Equations (5) and (6). When the $t \ll t_{\rm MAD}$, there is no magnetic jet torque braking the BH. Furthermore, the Bardeen (1970) accelerating hydrodynamic torque on the BH is larger than for an MAD (Lowell et al. 2023). This leads to a far greater equilibrium spin, $a_{\rm eq} = 1$. Thus, by having a long $t_{\rm MAD}$, the BH reaches a higher final spin. Solutions with $t_{\rm MAD} \geqslant t_f$ are excluded from the parameter space, since they would reach the MAD state after the mass reservoir is exhausted. We note that $\Phi(t)$ is a continuous function of t, and thus the magnetic flux on the engine and the jet power gradually increase until $\Phi(t)$ saturates. See Appendix B for the temporal evolution of solutions with high $t_{\rm MAD}$.

First-principles numerical simulations of collapsars (e.g., Gottlieb et al. 2022a, 2022b) show that the disk reaches the MAD state soon after the core collapse. If the disk does not become MAD early on, it energizes an expanding accretion shock that hampers magnetic flux on the disk such that the disk cannot become MAD at later times, disfavoring long $t_{\rm MAD}$. However, those simulations explored only a limited range of magnetic field profiles. It is possible that a low net magnetic flux within the star, or a magnetic flux profile that is concentrated far away from the core, would take a long time to saturate the central engine, leading to a long $t_{\rm MAD}$. Hence, $t_{\rm MAD}$ will depend on the initial magnetic field profile and the magnetic flux transport within the stellar envelope and the disk.

Figure 5 depicts the average jet power (panel (a)) and final BH spin (panel (b)) as a function of $\dot{m}$ and a_0 for $t_{\rm MAD} = 70$ s and $\chi = 1.5$. Fixing χ in Figure 5 leads to t_f being anticorrelated with $\dot{m}$, so high accretion rates lead to fast reservoir depletion. Thus, we exclude the solution with $\dot{m} \gtrsim 5 \times 10^{-2}\ M_\odot\ \mathrm{s}^{-1}$ as this entails $t_f \lesssim t_{\rm MAD}$.

In Figure 5(a), the white line delineates $R_{L_{\rm jet}} = 2.5$, above which are shown solutions with a low variation, $R_{L_{\rm jet}} < 2.5$. The red contours represent the observational 1σ spread around the average jet power (Goldstein et al. 2016). High jet power, $L_{\rm jet} \geqslant 5 \times 10^{51}$ erg s^{-1}, solutions with low variation are obtained above both contours and are weakly dependent on a_0. However, very high initial spins, $a_0 \gtrsim 0.4$, are excluded since they do not satisfy the variation constraint.

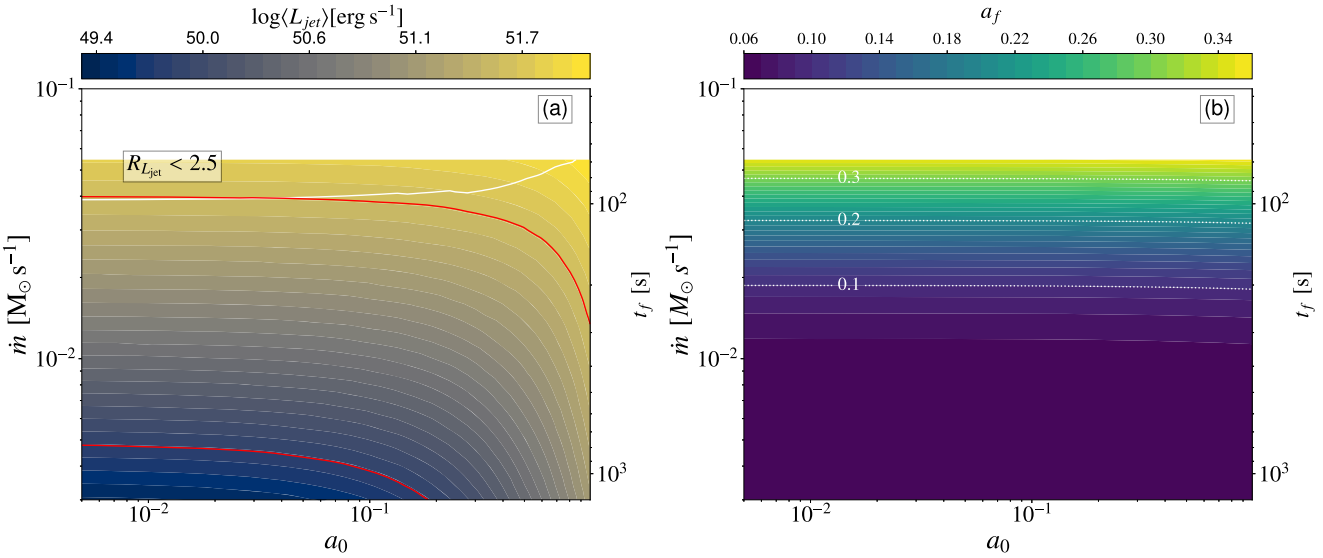

Figure 5. Effect of long $t_{\rm MAD} = 70$ s on the average jet power, $\langle L_{\rm jet}\rangle$ (panel (a)) and final spin, a_f (panel (b)) as functions of the accretion rate $\dot{m}$ and the initial spin, a_0. We assume $\chi = 1.5$ ($M_\star = 25\ M_\odot$, $M_0 = 2.5\ M_\odot$, $\lambda = 0.15$, and $R_\star = 1\ R_\odot$). The right axis displays the GRB duration t_f, using the accretion rate and χ from Equation (10). We do not plot solutions that have $t_{\rm MAD} > t_f$ (white area). Above the white contour lie the least variable jets, characterized by $R_{L_{\rm jet}} < 2.5$. The red lines constrain the observational 1σ spread around the average GRB jet power, assuming $\epsilon_\gamma = 0.5$. A large $t_{\rm MAD}$ allows for strong jets, $L_{\rm jet} \gtrsim 5 \times 10^{51}$ erg, while maintaining small variation, $R_{L_{\rm jet}}$, and small final spins, $a_f \leqslant 0.3$

In Figure 5(b), the maximum final spin $a_f \simeq 0.35$ is obtained at $t_f \simeq t_{\rm MAD}$, since the MAD state does not have enough time to spin down the BH. At longer t_f (lower $\dot{m}$), the BH can have a substantial spin down, and reach closer to $a = a_{\rm eq}$. Although the final spin is $a_f \lesssim 0.35$ or lower, it peaks at $a \simeq 0.6$ before spinning down. This peak is due to the Bardeen (1970) accelerating torque acting on the BH before $\Phi(t)$ saturates ($t < t_{\rm MAD}$). The peak in spin leads to a peak in jet power, so the jet reaches high energies while maintaining a low variation (see Appendix B). We conclude that delaying the jet activation to $\sim$70 s yields jets that are compatible with the most energetic GRBs.

5. Limitations

In Section 4 we use a semianalytic hydrodynamic model to solve the jet propagation in the star. On the one hand, Gottlieb et al. (2020) and Gottlieb & Nakar (2022) showed that weakly magnetized jets do not develop local hydrodynamical instabilities, and they propagate $\sim$2 times faster than their hydrodynamic counterparts. On the other hand, we consider strongly magnetized jets, which are subject to current-driven instabilities that may slow down the jets. In the absence of numerical modeling of the propagation of such jets, we adopted the numerical solution for hydrodynamic jets by Harrison et al. (2018). Nevertheless, in the companion paper (Gottlieb et al. 2023), we find that first-principles, strongly magnetized jets with a typical GRB power fail to retain their relativistic nature upon breakout, due to strong interactions with the star. This is in contrast to hydrodynamic and weakly magnetized models, which do not consider the tilt of the jet launching and kink instabilities. It is thus of utmost importance to generalize jet propagation models based on first-principles simulations.

We delay the activation of the jet by introducing the timescale by which the formation of the MAD is delayed post–core collapse, $t_{\rm MAD}$. However, we did not consider the engine-deactivation time, which we set at t_f, i.e., when the mass reservoir is exhausted. Magnetic field transport is responsible for the emergence or end of the MAD state (Tchekhovskoy et al. 2011). Once the magnetic flux saturates on the BH, the inner disk reaches the MAD state. The engine-deactivation time then depends on the magnetic field structure of the star and the magnetic field transport after and during the stellar collapse. Jacquemin-Ide et al. (2021) measured how the magnetic field transport depends on the strength of the initial magnetic field in accretion disks. However, how these results can be generalized to collapsars or to longer timescales is unclear, as the magnetic field transport mechanism remains poorly understood. Thus, the jet could turn off before t_f if the magnetic reservoir is exhausted or the magnetic structure reorganizes before t_f (Gottlieb et al. 2022a). Long-duration global collapsar simulations are needed to constrain the engine evolution on long timescales better.

Our model is built on 3D GRMHD simulations in which the disk is not cooled: they are meant to represent highly super-Eddington accretion systems (Lowell et al. 2023). This is also the case for the simulations of Gottlieb et al. (2022b, 2023). In reality, for the high accretion regimes of GRBs, neutrinos are the dominant cooling agent (e.g., Chevalier 1989; Batta & Lee 2014; Siegel et al. 2019). Cooling reduces the disk's geometric thickness, which may modify the magnetic and hydrodynamic spin-down torques that in turn could shift the equilibrium spin and the timescale on which the BH reaches that spin. Lowell et al. (2023) argued that thin accretion disks could lead to higher equilibrium spins, $a_{\rm eq} \sim 0.3$. Even though this value is larger than the one we consider by a factor of $\sim$3, it still is a relatively low spin. The biggest uncertainty that thin MADs introduce is the change in the efficiency of the spin-down torques. It is uncertain if a thin MAD requires a higher accreted mass to reach the equilibrium spin. Finally, Gottlieb et al. (2023) find an accretion rate that is not violent enough for neutrino cooling to be very strong for the mass accretion rates involved, so neutrino cooling might not considerably change our results.

The simulations of Gottlieb et al. (2023) show that the accretion rate, although slowly varying, is not entirely constant

Table 1
Required Parameters for Producing a Variety of GRB Luminosities

	Weak GRBs	Most GRBs	Strong GRBs
Average jet power	$\langle L_{\rm jet,obs}\rangle/\epsilon_\gamma \lesssim 6\times10^{49}$ erg s^{-1}	6×10^{49} erg s$^{-1}\lesssim\langle L_{\rm jet,obs}\rangle/\epsilon_\gamma\lesssim 4\times10^{51}$ erg s^{-1}	$\langle L_{\rm jet,obs}\rangle/\epsilon_\gamma \gtrsim 5\times10^{51}$ erg s^{-1}
Accretion rate	$\dot{m}\lesssim 2\times10^{-2}\ M_\odot$ s^{-1}	$2\times10^{-2}\ M_\odot$ s$^{-1}\lesssim \dot{\rm m}\lesssim 1.5\times10^{-1}$ M$_\odot$ s^{-1}	$\dot{m}\approx 3\times10^{-2}\ M_\odot$ s^{-1}
Accreted mass	$\chi\gtrsim 0.3$	$\chi\gtrsim 0.3$	$\chi\gtrsim 1.0$
MAD activation	$t_{\rm MAD}\ll t_f$	$t_{\rm MAD}\ll t_f$	$t_{\rm MAD}\sim t_f$, $t_{\rm MAD}<t_f$
Initial spin	$a_0\lesssim 0.1$	$a_0\lesssim 0.1$	$a_0\lesssim 0.4$

Note. The values of jet power are taken from Goldstein et al. (2016), and we assume a radiative efficiency $\epsilon_\gamma = 0.5$.

with time. Numerically, due to the limited simulation run time it is very hard to constrain the accretion rate on very long timescales. Furthermore, it is unclear how the spin down might affect the nonlinear feedback of jets on the accretion rate (Gottlieb et al. 2022a). Because of this, we do not include any temporal variation in the mass accretion rate in our model. In fact, when we include a slowly varying $\dot{m}$, we find that this makes it hard to satisfy the lack of variation in jet power suggested by observations (McBreen et al. 2002).

First-principles collapsar simulations feature wobbly jets (Gottlieb et al. 2022b), owing to the spontaneous tilt of the accretion disk. Such a wobble would alter the inferred jet energy from the one used in this paper. For example, if the tilt jet angle is 0.2 radians and its opening angle is 0.1 radians, then only 10% of the jet energy is observed for a given line of sight (Gottlieb et al. 2023). Thus, the presence of the wobble increases the total GRB jet energy by about an order of magnitude. Such an increase would favor solutions on the border of the parameter space shown in Figure 4, $\dot{m}\gtrsim 10^{-1}\ M_\odot$ s^{-1}, and long $t_{\rm MAD}$ values.

6. Conclusions

In this paper, we show that BH spin evolution to low spins is unavoidable in magnetically arrested collapsars. The final BH spin only weakly depends on the initial spin: it is primarily sensitive to the ratio between the total accreted mass and the BH mass at the onset of the MAD state. For physically motivated values of accreted mass, this results in a low BH spin. Achieving a high final spin is challenging even for conservative values of BH accretion of 20% of its initial mass, for which the final spin reaches $a_f\lesssim 0.1$.

Our model predicts that the spin distribution of post-GRB BHs will be centered around $a_{\rm eq}=0.07$, consistent with LVK measurements (Abbott et al. 2019; Wysocki et al. 2019; Callister et al. 2022; Tong et al. 2022; Abbott et al. 2023; Edelman et al. 2023). Furthermore, the LVK spin distributions show that highly spinning BHs, $a>0.7$, at least those that end up in merging binaries, should be rare or nonexistent (see however Galaudage et al. 2021). This suggests that the MAD spin-down mechanism may be relevant for LVK BHs. However, the impact of postnatal spin evolution channels, such as accretion and mergers, on the BH spin, remains to be seen.

If the post-GRB BH has a companion star, the relevance of a_f is a question of nature versus nurture. In other words, it is not clear whether the torques induced by the binary evolution of the BH binary system can wash out the post-GRB spin (Fishbach & Kalogera 2022). If not, our model could help in understanding the LVK BH spin distribution. If the post-GRB BH is isolated, subsequent mergers become relevant and could wash out the post-GRB spin. However, it is unknown whether most BHs are born from GRBs, and if they could be representative of the LVK population.

For consistency, we also check if our BH-powered jets are representative of typical GRBs and do not display any trends in their time evolution. In Table 1, we summarize the required mass accretion and MAD activation times for reproducing the variety of GRB powers. We find that most types of GRBs favor low initial spins, $a_0\leqslant 0.1$, thanks to their low variation, with the exception of strong jets, $\langle L_{\rm jet,obs}\rangle/\epsilon_\gamma\gtrsim 5\times10^{51}$ erg s^{-1}, which can display little variation up to a higher initial spin, $a_0\simeq 0.35$.

Our model predicts that the initial spin of the BH is likely slow, $a_0\leqslant 0.3$, as we also show in the companion paper (Gottlieb et al. 2023). This low initial spin for the central BH is consistent with new results using stellar evolution models (Fuller & Ma 2019; Belczynski et al. 2020). Indeed, considering efficient angular momentum transport between the stellar core and the envelope leads to a low initial spin. Nonetheless, the natal BH spin can still be high if jets are not launched (Fujibayashi et al. 2020, 2023). Furthermore, binary evolution may spin up the BH through rotational mixing, counteracting the efficient spin down of the Taylor instability. Indeed, Fuller & Ma (2019) found that in some cases of binary evolution the natal spin can reach high values of $a_0\sim 0.5$.

In this work, we assumed that the disk is in a magnetically arrested state. This assumption enables us to remove the freedom on the magnetic field strength, which can be coupled to the accretion rate. However, this assumption constrains our model to only GRBs that reach the MAD state. This is consistent with the simulations of Gottlieb et al. (2022a), which show that only BHs powered by MADs launch jets powerful enough to escape the stellar envelope. Thus, we do not believe that the MAD hypothesis is a stringent one. However, it is possible that other disk models could also produce GRBs, like magnetically elevated disks (Zhu & Stone 2018; Mishra et al. 2020; Jacquemin-Ide et al. 2021).

MADs are also known to launch magnetized disk winds through the Blandford & Payne (1982) process. This energy-extraction mechanism is treated self-consistently in our model, where the value of $l_{\rm HD}$ is lower than the standard value from Bardeen (1970) thanks to the action of this torque on the disk. MAD jets from rapidly spinning BHs are an order of magnitude more energetic than their disk winds. However, this is not the case for slowly spinning BHs, for which the jets are much weaker than that from a fast-spinning BH (Tchekhovskoy et al. 2012; Tchekhovskoy & McKinney 2012; Sadowski et al. 2013; Tchekhovskoy 2015). At lower spins, $a\lesssim 0.3$, the winds outshine the jets. Nevertheless, the observed prompt emission is still solely related to the jet energetics since the jet's collimation facilitates their propagation to break out faster than the more isotropic winds (Gottlieb et al. 2023). It remains to be

seen what happens when $a_0 \approx 0$, where the winds are launched before the BH spins up to $a_{\rm eq}$.

In a companion paper (Gottlieb et al. 2023), we show that a slowly spinning BH, with $a_0 \simeq 0.2$, generates jets with typical GRB powers. GRBs with higher initial spins would exhibit too much variation. Weak GRBs can be explained by $\dot{m} \lesssim 2 \times 10^{-2}\ M_\odot\ {\rm s}^{-1}$, at a low initial spin, $a_0 < 0.1$ (see Figure 4). In order to obtain low variation for powerful GRB jets, we introduce a delayed jet activation time, $t_{\rm MAD} \sim t_f$. This allows the BH to spin up during the first stage of accretion in the absence of jet activity. The rapidly spinning BH then powers a strong jet, and ultimately spins down to $a_f \lesssim 0.3$. A long $t_{\rm MAD}$ could be the consequence of a star with a weak magnetic field or a magnetic flux that has a steep radial profile, see Section 4.2.

Acknowledgments

We thank Enrico Ramirez-Ruiz for his thoughtful comments. We thank both referees for thoughtful suggestions that have helped to improve the manuscript. J.J. and A.T. acknowledge support by the NSF AST-2009884 and NASA 80NSSC21K1746 grants. O.G. is supported by a CIERA Postdoctoral Fellowship. O.G. and A.T. acknowledge support by Fermi Cycle 14 Guest Investigator program 80NSSC22K0031. B.L. acknowledges support by a National Science Foundation Graduate Research Fellowship under grant No. DGE-2234667. B.L. also acknowledges support by an Illinois Space Grant Consortium (ISGC) Graduate Fellowship supported by a National Aeronautics and Space Administration (NASA) grant awarded to the ISGC. A.T. was also supported by NSF grants AST-2107839, AST-1815304, AST-1911080, AST-2206471, and OAC-2031997, and NASA grant 80NSSC18K0565. Support for this work was also provided by the National Aeronautics and Space Administration through Chandra Award Number TM1-22005X issued by the Chandra X-ray Center, which is operated by the Smithsonian Astrophysical Observatory for and on behalf of the National Aeronautics Space Administration under contract NAS8-03060. This research used resources of the Oak Ridge Leadership Computing Facility, which is a DOE Office of Science User Facility supported under Contract DE-AC05-00OR22725. An award of computer time was provided by the ASCR Leadership Computing Challenge (ALCC), Innovative and Novel Computational Impact on Theory and Experiment (INCITE), and OLCF Director's Discretionary Allocation programs under award PHY129. This research used resources of the National Energy Research Scientific Computing Center, a DOE Office of Science User Facility supported by the Office of Science of the U.S. Department of Energy under Contract No. DE-AC02-05CH11231 using NERSC award ALCC-ERCAP0022634.

Data Availability

The data underlying this article will be shared upon reasonable request to the corresponding author.

Appendix A
Comparison with the Spin-down Model

We compute the spin-up parameter using our semianalytic model (Equation (7)) for two collapsar simulations. One simulation has a BH spin $a = 0.8$ from Gottlieb et al. (2022b), and we conduct an additional identical simulation, but with $a = 0.1$. We compare the results with the MAD spin-down model from Lowell et al. (2023), which was calibrated by the GRMHD simulations initialized with a gaseous torus. We can calculate s using

$$s = l - 2ae, \tag{A1}$$

where l and e are the angular momentum and energy fluxes, respectively, onto the BH.

In Figure 6, we plot the spin-up parameter versus time for the two simulations. We calculate the average s for the $a = 0.8$ simulation after $t_{\rm MAD}$ and find $s_{\rm avg} \approx -6.5$. For the $a = 0.1$ simulation, after $t = 1$ s we find $s_{\rm avg} \approx -0.2$. We show the values of s from the MAD spin-down model, $s_{\rm model}$, with horizontal dashed lines. For $a = 0.1$, the model gives $s_{\rm model} = -0.4$, a factor of $\sim$2 difference, and for $a = 0.8$, it gives $s_{\rm model} = -7.5$, a 15% difference. We believe that the weaker spin simulation shows a larger deviation because it is closer to the equilibrium spin, $a_{\rm eq} = 0.07$. Hence, the spin-up parameter, s, is oscillating close to 0 and might reach positive values that hinder the average. Furthermore, a factor of $\sim$2 is a small error when compared with the other uncertainties of the model, e.g., accretion rate and magnetic field evolution. We can conclude that the spin evolution model is consistent with collapsar simulations, showing that the MAD spin evolution model can be used for GRBs.

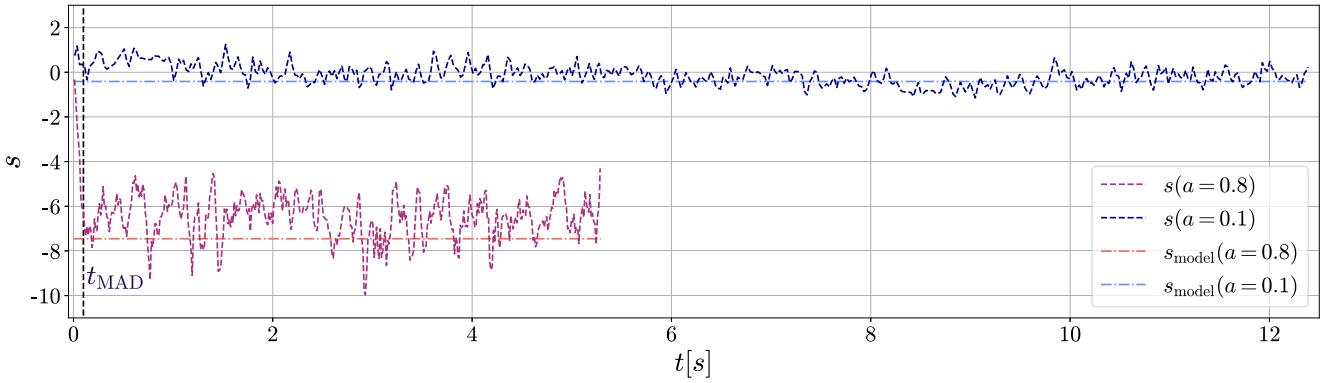

Figure 6. Spin-up parameter vs. time for collapsar simulations with BH spin values of $a = 0.1$ and $a = 0.8$. The pink and dark blue dashed lines show moving averages of s for $a = 0.8$ and $a = 0.1$, respectively. The horizontal orange and light blue lines show the values calculated from the MAD model for $a = 0.8$ and $a = 0.1$, respectively. The time where the system reaches the MAD state in the $a = 0.8$ simulation, $t_{\rm MAD}$, is shown by the vertical black line.

Appendix B
The Effects of Delaying the Onset of the MAD State

Figures 7(a) and (b) show the jet power and spin profiles for different a_0 for $t_{\rm MAD} = 60$ s. The left and right triangles in panel (b) show t_1 and t_2, between which the maximal spin and jet luminosity emerge. The spin-down torque starts to act well before $t_{\rm MAD}$ because the spin-down torque activates smoothly, mimicking a continuous build up of the magnetic flux on the central BH. The observed jet power is dominated by the time during which the BH spins at $a \sim 0.6$. The solutions still have a low variation, $R_{L_{\rm jet}} < 2.5$.

Figure 7(c) displays the final spins as a function of $1/\chi$ and $t_{\rm MAD}$ for an initial spin of $a_0 = 0.9$. In order to achieve high final spins, $a_f \simeq 0.6$, χ needs to be small and $t_{\rm MAD} \gtrsim 10$ s. Thus, high final spins can be obtained, but require a total accreted mass that is largely inconsistent with the mass gap argument.

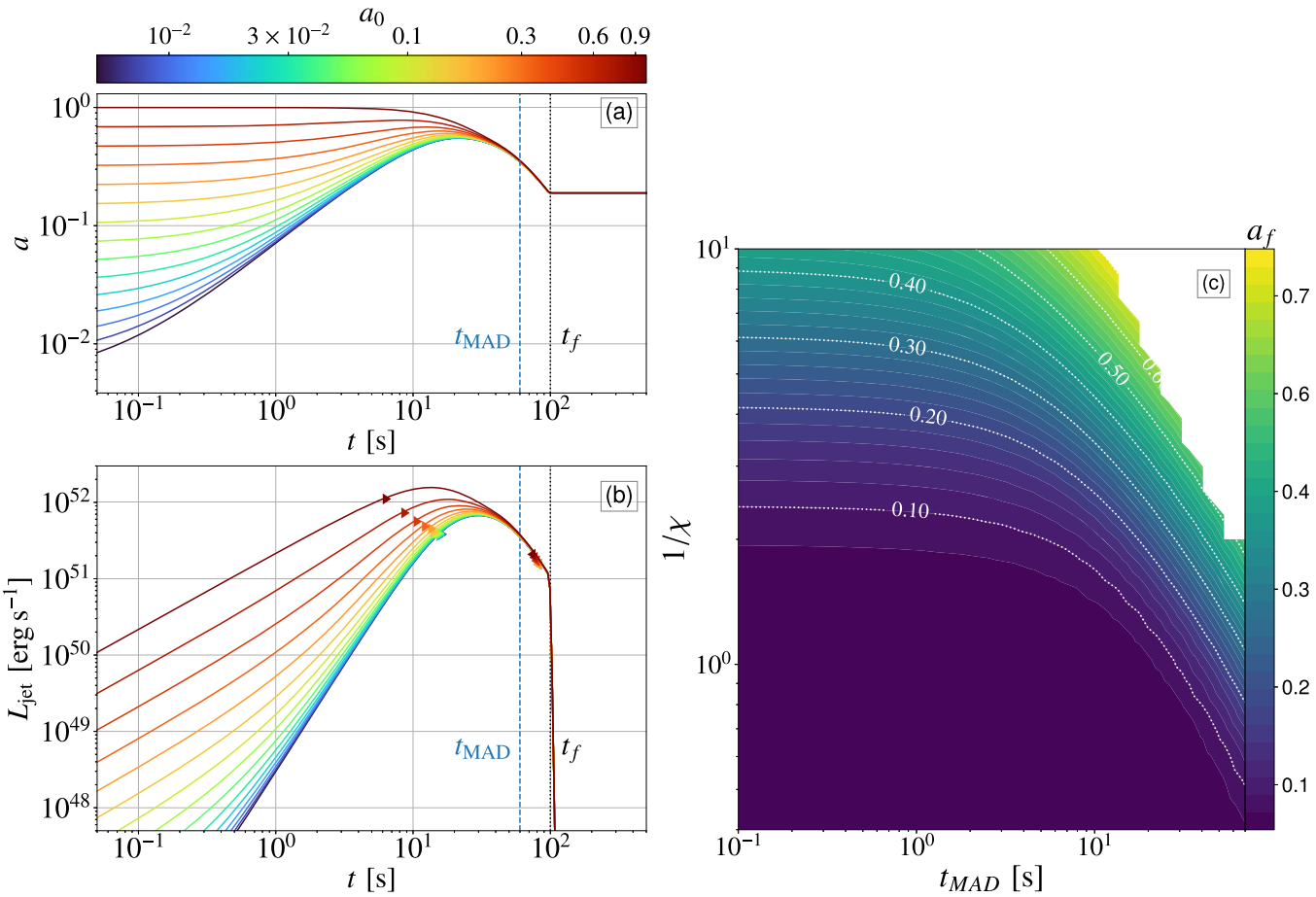

Figure 7. Evolution of a (panel (a)) and $L_{\rm jet}$ (panel (b)) as functions of time and different initial spins $a_0 \in [5 \times 10^{-3}, 1.0]$. We also plot t_f (black) and $t_{\rm MAD}$ (blue) as vertical lines. The left and right triangles in panel (b) represent t_1 and t_2, respectively. (c) Final spin, a_f, as a function of $1/\chi$ and the MAD activation timescale, $t_{\rm MAD}$ computed for an initial spin $a_0 = 0.9$. We do not show solutions that have $t_{\rm MAD} > t_f$. For $\chi \geqslant 0.5$, the MAD activation timescales do not affect the final spin considerably. A high $t_{\rm MAD}$ leads to a higher jet power without considerably modifying the final spin.

ORCID iDs

Jonatan Jacquemin-Ide https://orcid.org/0000-0003-2982-0005
Ore Gottlieb https://orcid.org/0000-0003-3115-2456
Beverly Lowell https://orcid.org/0000-0002-2875-4934
Alexander Tchekhovskoy https://orcid.org/0000-0002-9182-2047

References

Abbott, B. P., Abbott, R., Abbott, T. D., et al. 2019, ApJL, 882, L24
Abbott, R., Abbott, T. D., Abraham, S., et al. 2020, ApJL, 896, L44
Abbott, R., Abbott, T. D., Acernese, F., et al. 2023, PhRvX, 13, 011048
Aloy, M. Á., & Obergaulinger, M. 2021, MNRAS, 500, 4365
Bailyn, C. D., Jain, R. K., Coppi, P., & Orosz, J. A. 1998, ApJ, 499, 367
Bardeen, J. M. 1970, Natur, 226, 64
Batta, A., & Lee, W. H. 2014, MNRAS, 437, 2412
Belczynski, K., Klencki, J., Fields, C. E., et al. 2020, A&A, 636, A104
Belczynski, K., Wiktorowicz, G., Fryer, C. L., Holz, D. E., & Kalogera, V. 2012, ApJ, 757, 91
Bethe, H. A. 1990, RvMP, 62, 801
Bisnovatyi-Kogan, G. S., & Ruzmaikin, A. A. 1974, Ap&SS, 28, 45
Bisnovatyi-Kogan, G. S., & Ruzmaikin, A. A. 1976, Ap&SS, 42, 401
Blandford, R. D., & Payne, D. G. 1982, MNRAS, 199, 883
Blandford, R. D., & Znajek, R. L. 1977, MNRAS, 179, 433
Bromberg, O., Nakar, E., Piran, T., & Sari, R. 2011, ApJ, 740, 100
Callister, T. A., Miller, S. J., Chatziioannou, K., & Farr, W. M. 2022, ApJL, 937, L13
Chan, C., Müller, B., Heger, A., Pakmor, R., & Springel, V. 2018, ApJL, 852, L19
Chevalier, R. A. 1989, ApJ, 346, 847
Edelman, B., Farr, B., & Doctor, Z. 2023, ApJ, 946, 16
Farr, W. M., Sravan, N., Cantrell, A., et al. 2011, ApJ, 741, 103
Farr, W. M., Stevenson, S., Miller, M. C., et al. 2017, Natur, 548, 426
Fishbach, M., & Kalogera, V. 2022, ApJL, 929, L26
Fujibayashi, S., Sekiguchi, Y., Shibata, M., & Wanajo, S. 2023, ApJ, 956, 100
Fujibayashi, S., Shibata, M., Wanajo, S., et al. 2020, PhRvD, 102, 123014
Fuller, J., & Ma, L. 2019, ApJL, 881, L1
Galaudage, S., Talbot, C., Nagar, T., et al. 2021, ApJL, 921, L15
Gal-Yam, A., Bruch, R., Schulze, S., et al. 2022, Natur, 601, 201
García, J., Dauser, T., Lohfink, A., et al. 2014, ApJ, 782, 76
Goldstein, A., Connaughton, V., Briggs, M. S., & Burns, E. 2016, ApJ, 818, 18
Gottlieb, O., Bromberg, O., Singh, C. B., & Nakar, E. 2020, MNRAS, 498, 3320
Gottlieb, O., Jacquemin-Ide, J., Lowell, B., Tchekhovskoy, A., & Ramirez-Ruiz, E. 2023, ApJL, 952, L32
Gottlieb, O., Lalakos, A., Bromberg, O., Liska, M., & Tchekhovskoy, A. 2022a, MNRAS, 510, 4962
Gottlieb, O., Liska, M., Tchekhovskoy, A., et al. 2022b, ApJL, 933, L9
Gottlieb, O., Nagakura, H., Tchekhovskoy, A., et al. 2023, ApJL, 951, L30
Gottlieb, O., & Nakar, E. 2022, MNRAS, 517, 1640
Halevi, G., Wu, B., Moesta, P., et al. 2023, ApJ, 944, L38
Harrison, R., Gottlieb, O., & Nakar, E. 2018, MNRAS, 477, 2128
Hoy, C., Fairhurst, S., Hannam, M., & Tiwari, V. 2022, ApJ, 928, 75
Jacquemin-Ide, J., Lesur, G., & Ferreira, J. 2021, A&A, 647, A192
Janiuk, A., Moderski, R., & Proga, D. 2008, ApJ, 687, 433
Komissarov, S. S., & Barkov, M. V. 2009, MNRAS, 397, 1153
Kovetz, E. D., Cholis, I., Breysse, P. C., & Kamionkowski, M. 2017, PhRvD, 95, 103010
Leng, M., & Giannios, D. 2014, MNRAS, 445, L1
Liu, T., Hou, S.-J., Xue, L., & Gu, W.-M. 2015, ApJS, 218, 12
Lowell, B., Jacquemin-Ide, J., Tchekhovskoy, A., & Duncan, A. 2023, arXiv:2302.01351
Lyutikov, M., & Blandford, R. 2003, arXiv:astro-ph/0312347
MacFadyen, A. I., & Woosley, S. E. 1999, ApJ, 524, 262
Mandel, I., Farr, W. M., Colonna, A., et al. 2017, MNRAS, 465, 3254
Margalit, B., & Metzger, B. D. 2017, ApJL, 850, L19
McBreen, S., McBreen, B., Hanlon, L., & Quilligan, F. 2002, A&A, 393, L29
McClintock, J. E., Narayan, R., & Steiner, J. F. 2014, SSRv, 183, 295
Middleton, M. 2016, in Astrophysics of Black Holes: From Fundamental Aspects to Latest Developments, ed. C. Bambi (Berlin: Springer)
Mishra, B., Begelman, M. C., Armitage, P. J., & Simon, J. B. 2020, MNRAS, 492, 1855
Moderski, R., & Sikora, M. 1996, MNRAS, 283, 854
Narayan, R., Chael, A., Chatterjee, K., Ricarte, A., & Curd, B. 2022, MNRAS, 511, 3795
Narayan, R., Igumenshchev, I. V., & Abramowicz, M. A. 2003, PASJ, 55, L69
Obergaulinger, M., & Aloy, M. Á. 2022, MNRAS, 512, 2489
Özel, F., Psaltis, D., Narayan, R., & McClintock, J. E. 2010, ApJ, 725, 1918
Penrose, R., & Floyd, R. M. 1971, NPhS, 229, 177
Reynolds, C. S. 2021, ARA&A, 59, 117
Roulet, J., & Zaldarriaga, M. 2019, MNRAS, 484, 4216
Sądowski, A., Narayan, R., Penna, R., & Zhu, Y. 2013, MNRAS, 436, 3856
Shapiro, S. L., & Shibata, M. 2002, ApJ, 577, 904
Shibata, M., & Shapiro, S. L. 2002, ApJL, 572, L39
Siegel, D. M., Barnes, J., & Metzger, B. D. 2019, Natur, 569, 241
Tchekhovskoy, A. 2015, in The Formation and Disruption of Black Hole Jets, ed. I. Contopoulos, D. Gabuzda, & N. Kylafis (Cham: Springer)
Tchekhovskoy, A., & McKinney, J. C. 2012, MNRAS, 423, L55
Tchekhovskoy, A., McKinney, J. C., & Narayan, R. 2012, JPhCS, 372, 012040
Tchekhovskoy, A., Narayan, R., & McKinney, J. C. 2010, ApJ, 711, 50
Tchekhovskoy, A., Narayan, R., & McKinney, J. C. 2011, MNRAS, 418, L79
Tiwari, V., Fairhurst, S., & Hannam, M. 2018, ApJ, 868, 140
Tong, H., Galaudage, S., & Thrane, E. 2022, PhRvD, 106, 103019
Woosley, S. E. 1993, ApJ, 405, 273
Wysocki, D., Lange, J., & O'Shaughnessy, R. 2019, PhRvD, 100, 043012
Zhang, S. N., Cui, W., & Chen, W. 1997, ApJL, 482, L155
Zhu, Z., Johnson, M. D., & Narayan, R. 2019, ApJ, 870, 6
Zhu, Z., & Stone, J. M. 2018, ApJ, 857, 34